H_∞ control of a redox flow battery considering the effect of overpotentials

Alejandro Clemente
Institut de Robòtica i Informàtica Industrial
Universitat Politècnica de Catalunya
Barcelona, Spain
alejandro.clemente.leon@upc.edu

Ramon Costa-Castelló
Institut de Robòtica i Informàtica Industrial
Universitat Politècnica de Catalunya
Barcelona, Spain
ramon.costa@upc.edu

Abstract—**This conference paper presents a comparison between a H_∞ control technique and a classical PID, applied on a redox flow battery system. The study presents a dynamic nonlinear electrochemical model that considers the effect of overpotentials losses in the computation of the voltage measurement. The H_∞ controller is designed to regulate the output voltage of the battery considering specific fit criteria. Moreover, this controller is compared with a classic PID controller commonly used in the industry. To ensure the same imposed adjustment criteria of the classic controller, a particle swarm optimizer method is used to find it. Finally, a comparison between the designed H_∞ controller, and the classic PID found through optimization is presented.**

Index Terms—**Redox flow battery, H_∞ control, Particle Swarm Optimization**

I. INTRODUCTION

Nowadays, the rise of renewable energies has more and more weight within the energy situation, existing a trend towards the use of clean and renewable energy. Especially, the use of solar and wind power has become ones of the most demanded sources of energy today. On the one hand, wind energy provide most of the renewable electricity in the world with a percentage of 35%. On the other hand, solar energy has become the fastest-growing energy source reaching a 13% of the total renewable energy, very far from 1% generated in 2008 [1]. However, there is a limitation in their use due to its dependence on weather conditions, making necessary the use of energy storage systems (ESS) [2].

There exist different types of ESS depending on the mechanisms used to transform and store energy, being the redox flow battery (RFB) one of the most promising techniques, especially for large-energy storage, making them optimal for implementation in solar or wind plants [3]. Furthermore, they can also be used within microgrids as energy storage equipment [4]. Within the field of RFB systems, the all vanadium redox flow battery (VRFB) introduced by Skyllas-Kazacos [5], has become the best option due to its great advantages over other types of electrolytes, as the possible mixture of electrolytes, its long cycle life and high energy efficiency [6].

Considering that VRFB is a relatively new technology, there exist a lot of study done on it, covering different important aspects. Most of the literature is focused on the estimation of certain parameters and variables, such as the determination of the state of charge (SOC) and more recently the state of health (SOH) [7]. Another important point of study and analysis within the VRFB, is the correct choice of the charging technique, seeking a compromise between safety and reliability.

Most of the studies found in the literature, present a charging technique that consists on charging the battery using a constant current-voltage (CC-CV) and a constant flow rate [8]. One of the most used techniques consist on first charging the battery using a constant current, followed by a constant voltage when it is near to the maximum SOC [9]. The aim of this technique is to charge the battery in a quickly and safely manner, avoiding the appearance of gassing side reactions. These gassing side reactions can damage the system, reducing the battery capacity. On the one hand, the positive electrode can be damaged by the appearance of CO_2 and O_2 [10]. On the other hand, the negative electrode can suffer from H_2 gas generation [11]. The generation of these gases in both electrodes, is directly related with the rapidly increase of terminal voltage, and for that reason charging the battery at a constant current can lead to operation problems for the system.

Considering this issue, a new control strategy is needed. One solution, consists on varying the electrolyte flow rate to ensure a constant terminal voltage that do not undergo secondary reactions, and can be constant even though the current presents sudden changes in its absolute value. A control strategy for the terminal voltage is proposed in [12], that consists on a H_∞ controller considering abrupt changes in current. However, it only uses the Nernst equation and does not take into account the effect of the existent over-potentials. Furthermore, in the literature there is not a comparison between different control strategies for the intended purpose in VRFB systems.

An important factor for the development of a control strategy, is the selection of a model that must be as realistic as possible to it into a real system easily. Regarding models for VRFB, usually is assumed that the concentration is the same in all parts of the system. This assumption is only valid

if the flow rate is sufficiently high, making practically equal the concentration inside the cell and the tanks [13]. However, for control strategies that require a variable flow rate, this condition is not always ensured, so a model that differentiates between the concentration in the tank and the cell is necessary. Moreover, in order to obtain a realistic estimation of the terminal voltage, the effect of different over-potentials must be considered. The activation over-potential, which is calculated using the Butler-Volmer equation, can be simplified to the Tafel equation [14]. Nevertheless, this simplification can lead to significant errors [15] depending on the current magnitude. Hence, a simple expression with less error is presented to take into account the effect of this over-potential in the model.

Consequently to the different aspects presented, this work proposes a control strategy capable to ensure a desired output voltage, regardless of the current imposed by the grid in the charging process, or by the load in the discharge ones. One of the novelties yields on the use of a nonlinear dynamic model that differentiates between species concentrations in different parts of the system, and presents a more exact expression for the output voltage. To guarantee the correct operation of the controller throughout the total operational range, the H_∞ technique is used, taking into account all possible operating points of the linearized model. A comparison between this technique and a PID tuned by means of a Particle Swarm Optimizer (PSO) is presented, to highlight the advantages of the proposed method, with respect to a classic controller highly used in the industry.

The work is organized as follows: Section II presents the dynamic nonlinear model with the expression of the output voltage. Starting from the model, the design of the H_∞ controller is presented in Section III. A PSO method is explained in Section IV that allows to obtain a PID controller based in the desired criteria of performance. Section V analyze the main results of both H_∞ and classic PID controllers, while Section VI presents a comparative evaluation. Finally, the fruitful conclusions appear summarized in Section VII.

II. MODEL FORMULATION

There exist different models in the literature that define the behaviour of a VRFB. Among all existing ones, the dynamic electrochemical model of Skyllas Kazacos [16], who was pioneer in the use of vanadium for RFB, is the ones most used, presenting a compromise in terms of reality fitting and simplicity. Based on its model, it is possible to express the evolution of each vanadium species (V^{2+},V^{3+},VO^{2+} and VO_2^+) inside the cell and tanks, and use them to define the variables of interest of the system, which are the output voltage (which only depends on the cell concentration) and the SOC (that depends on tanks concentration).

A. Dynamic concentration model

The evolution of the concentration of each vanadium species can be represented in the state-space as:

$$\dot{\boldsymbol{x}} = \mathbf{A}\boldsymbol{x} + \mathbf{B}\boldsymbol{x} \cdot q + \mathbf{b}j \tag{1}$$

being $\boldsymbol{x}=[c_2^c, c_3^c, c_4^c, c_5^c, c_2^t, c_3^t, c_4^t, c_5^t]^T$ the state vector of species concentration, where the sub-index expresses the vanadium species (2 for V^{2+}, 3 for V^{3+}, 4 for VO^{2+} and 5 for VO_2^+) and the super-index indicates where is it located (c for the cell and t for the tank). The inputs of the system are the the current density j and the flow rate q. All system parameters are defined by matrices $\mathbf{A}$, $\mathbf{B} \in \mathbb{R}^{8\times8}$ that are related with the diffusion and flow rate, respectively, and the vector $\mathbf{b} \in \mathbb{R}^8$ that contains the system parameters of the charging/discharging current effect. All model arrays appear summarized in the Appendix section.

B. SOC computation

The SOC of a VRFB gives information about the percentage of energy stored in the system, and is directly related with the concentration of vanadium species inside the tanks. Considering that the evolution of species concentration in the anolyte and catholyte can be different, there exist a distinction:

$$SOC_- = \left(\frac{x_5}{x_5 + x_6} \right) \tag{2}$$

$$SOC_+ = \left(\frac{x_8}{x_7 + x_8} \right). \tag{3}$$

where SOC_- and SOC_+ compute the SOC in the anolyte and catholyte reservoirs of the system, respectively. In practice, the real SOC of the system would correspond to the minimum of them, determining the maximum energy that can be stored.

C. Output voltage computation

As with other types of batteries or fuel cells, the VRFB voltage can be computed by means of the Nersnt equation (V^{nernst}) and considering the different over-potentials (η) and the formal electrode potential (V^θ). In this way, the following expression can be formulated:

$$V = V^\theta + V^{nernst} + \eta \tag{4}$$

where experimentally it has been seen that the formal potential V^θ has a value of 1.4V [17]. The V^{nernst} is computed taking into account the concentration of vanadium species and the hydrogen protons (c_{H_+}) formed in the catholyte:

$$V^{nernst} = \frac{RT}{F} \cdot ln \left[\left(\frac{x_4 \cdot c_{H_+}^2}{x_3} \right)_{catholyte} \left(\frac{x_1}{x_2} \right)_{anolyte} \right] \tag{5}$$

where R is the gas constant, F is the Faraday constant and T is the temperature of the cell/stack. The formation of protons in the catholyte can be expressed as follows:

$$c_{H+} = c_{H+}(0) + x_4 \tag{6}$$

where $c_{H+}(0)$ represents the initial concentration of hydrogen protons, that exist due to the presence of sulphuric acid in the composition of the electrolytes.

An important factor to consider in the computation of the cell/stack voltage is the effect of the different over-potentials. Like other similar batteries, there are different types of losses,

being the ohmic and activation losses the most important within the VRFB.

On the one hand, the ohmic over-potential (η^{ohm}) can be formulated as follow:

$$\eta^{ohm} = r \cdot j \cdot s_e, \tag{7}$$

where r is the cell/stack resistance and s_e is the electrode surface.

On the other hand, the activation over-potential (η^{act}) expression can be formulated by means of the Butler-Volmer equation considering no mass-transfer effect (electrode surface concentrations do not differ from bulk values) [18]:

$$j = j_0 \left(e^{\dfrac{(1-\alpha) \cdot F}{R \cdot T} \eta^{act}} - e^{-\dfrac{\alpha \cdot F}{R \cdot T} \eta^{act}} \right) \tag{8}$$

being j_0 the exchange current density at equilibrium and α the change transfer coefficient.

The exchange current density depends on the species concentration inside the cell and the rate constant k^θ, and can be computed as follows:

$$j_0 = \frac{1}{s_e} \cdot \left(F \cdot k^\theta \cdot x_1^{1-\alpha} \cdot x_2^\alpha \cdot x_3^\alpha \cdot x_4^{1-\alpha} \right) \tag{9}$$

As can be noticed, the term η^{act} only depends on the current density and the exchange current density. On the one hand, the current density is easy to measure, as it is imposed by the user. On the other hand, the exchange current density can be determined by the specie concentration inside the cell. Although it cannot be measured directly, by means of an observer its value can be estimated [19]. However, (8) defines a smooth implicit function $\eta^{act}(j, j_0, \alpha)$ that cannot be numerically isolated.

In this work, considering that the values of α are near to 0.5, it has been decided to define a 3 piecewise function using the linear and hyperbolic sine approximations [20].

Therefore, for low values of $|\eta^{act}|$ the linear approximation will be used, and for large values of η^{act} the hyperbolic sine function. It has been found that the limit of η^{act} is near 30 mV depending on the value of α. Fig. 1 shows the corresponding 3 piecewise function for $\alpha = 0.51$, where it is shown the relation between η^{act} and the current/exchange current density term (j/j_0). The red trace defines the original Butler-Volmer expression, the blue trace defines the linear approximation considering a value of $\alpha = 0.5$, and black and green traces define the hyperbolic sine approximation for charging and discharging currents, respectively.

Considering that the linear approximation can be simplified taking into account the positive term, it is possible to formulate
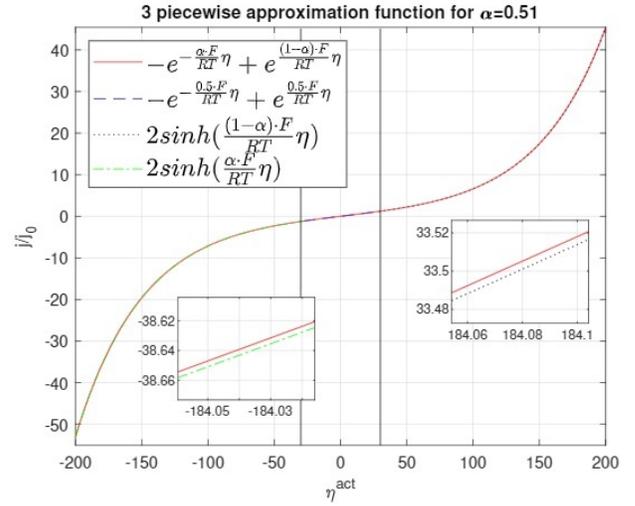

Fig. 1. 3 piecewise approximation for α=0.51.

in a compact form the activation over-potential expression:

$$\eta^{act} = \begin{cases} \dfrac{R \cdot T}{(1-\alpha)F} hsin^{-1}\left(\dfrac{j}{j_0}\right) & \text{if } j/j_0 < lb \\[2mm] \dfrac{R \cdot T}{0.5 \cdot F} ln\left(\dfrac{j}{j_0}\right) & \text{if } lb < j/j_0 < ub \\[2mm] \dfrac{R \cdot T}{\alpha \cdot F} hsin^{-1}\left(\dfrac{j}{j_0}\right) & \text{if } j/j_0 > ub \end{cases} \tag{10}$$

where lb and ub are the lower and upper bounds, respectively, that define the extreme values of the linear approximation. For the example shown in Fig 1 the lower and upper bounds are in -30 mV and 30 mV, which correspond to -2 and 2 for the term j/j_0.

Therefore, the expression of the over-potential (η) can be formulated considering (7) and (10) as:

$$\eta = \eta^{ohm} + \eta^{act} \tag{11}$$

By substituting (11) in (4) the global expression of the output voltage is achieved.

III. H_∞ CONTROL DESIGN

This section presents the design of the H_∞ controller that will be used to control the output voltage of a VRFB. The procedure follows a theory formulation that allow to specify the performance and stability conditions of the desired controller.

This theory design is based on the use of the infinity norm $||\cdot||_\infty$, that makes possible to define the desired specifications of the controller [21]. By means of different weighting functions is possible to specify the stability of the system and the desired performance. One of the advantages of the use of the $||\cdot||_\infty$ is that makes possible to formulate the design as an optimization problem, where the solution is the H_∞ controller that best fulfills with the desired characteristics. Moreover, one of the most important advantages is that can deal with

uncertainty if it is well modeled and defined. The procedure can be summarized in the following steps:

1) Linearize the system
2) Modeling the uncertainty considering all possible operating conditions
3) Design the controller by means of $\| \cdot \|_\infty$ formulation.
4) Introducing an integral action to cancel steady state error.

A. System linearization

The VRFB system can be computed by means of (1) that defines the state space part, and (4) which defines the output. Due to the nonlinearity of the output voltage expression, the system can be rewritten in the following nonlinear form:

$$\dot{\boldsymbol{x}} = f(\boldsymbol{x}, \boldsymbol{u})$$
$$y = h(\boldsymbol{x}, \boldsymbol{u}) \tag{12}$$

where f is defined by matrices $\mathbf{A}$, $\mathbf{B}$ and $\mathbf{b}$ which are linear, and h defines the nonlinear V expression. Both terms depend on the state space vector $\boldsymbol{x}$ and the input vector $\boldsymbol{u} = [q, j]$.

A nonlinear system in the form (12) can be linearized by means of the Taylor expansion, obtaining the following formulation:

$$\Delta \dot{\boldsymbol{x}} = \mathcal{A}\Delta \boldsymbol{x} + \mathcal{B}\Delta \boldsymbol{u}$$
$$\Delta y = \boldsymbol{c}\Delta \boldsymbol{x} + \boldsymbol{d}\Delta \boldsymbol{u} \tag{13}$$

where $\Delta \boldsymbol{x} = \boldsymbol{x} - \bar{\boldsymbol{x}}$, $\Delta \boldsymbol{u} = \boldsymbol{u} - \bar{\boldsymbol{u}}$ and $\Delta y = y - \bar{y}$, being $\bar{\boldsymbol{x}}$, $\bar{\boldsymbol{u}}$ and $\bar{y}$ the equilibrium points of the different variables. The matrices $\mathcal{A}$, $\mathcal{B}$, $\boldsymbol{c}$ and $\boldsymbol{d}$ are computed by means of the Jacobian as:

$$\mathcal{A} = \left.\frac{\partial f}{\partial \boldsymbol{x}}\right|_{\bar{\boldsymbol{x}},\bar{\boldsymbol{u}}} \quad \mathcal{B} = \left.\frac{\partial f}{\partial \boldsymbol{u}}\right|_{\bar{\boldsymbol{x}},\bar{\boldsymbol{u}}} \quad \boldsymbol{c} = \left.\frac{\partial h}{\partial \boldsymbol{x}}\right|_{\bar{\boldsymbol{x}},\bar{\boldsymbol{u}}} \quad \boldsymbol{d} = \left.\frac{\partial h}{\partial \boldsymbol{u}}\right|_{\bar{\boldsymbol{x}},\bar{\boldsymbol{u}}}$$

As can be noticed, f is linear in the model described in (1) so matrices $\mathcal{A}$ and $\mathcal{B}$ become:

$$\mathcal{A} = \mathbf{A} + \mathbf{B}\bar{u}_1 \tag{14}$$
$$\mathcal{B} = \mathbf{B}\bar{x} + \mathbf{b} \tag{15}$$

For the case of $\boldsymbol{c}$ and $\boldsymbol{d}$ computation, mathematical analysis is needed to perform the Jacobian of the nonlinear voltage equation, appearing summarized in the Appendix section.

B. Uncertainty modeling

According to (13) the different arrays and matrices ($\mathcal{A}$,$\mathcal{B}$, $\boldsymbol{c}$, and $\boldsymbol{d}$) that composed the linearized system depend on the state variables $\boldsymbol{x}$ and the inputs $\boldsymbol{u}$.

Considering a total vanadium concentration c_v of 0.4 M, the possible values of vanadium species concentration $\boldsymbol{x}$ are limited within the range of 0 to 400 mol/m^3. For the case of the inputs variables, operational ranges have also been defined. On the one hand, for the case of the current density, it has been selected a range between 0 and 300 mA/cm^2. On the other hand, the flow rate can vary between 10 ml/min to 200 ml/min. Taking into account these ranges, it has been possible to obtain the frequency response of the model
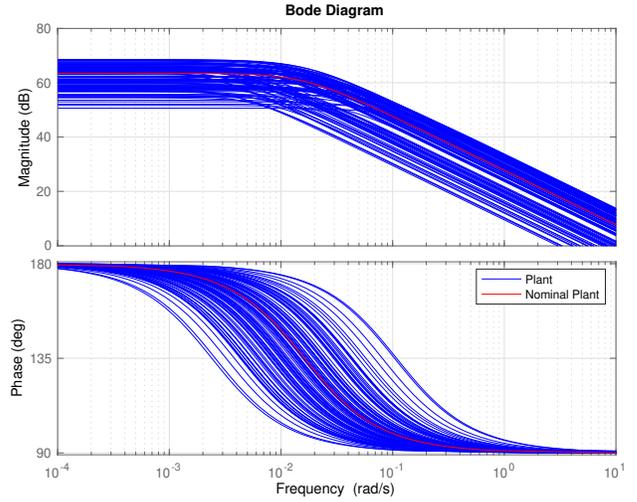

Fig. 2. Bode Diagram for different linear plants in the operational range.

considering all different plants. Fig. 2 shows the variability of the model considering the operational conditions selected.

The aim of this work, is propose a controller that is capable of controlling the voltage throughout the operational range. Therefore, an uncertainty model has been designed, considering an additive uncertainty that can be introduce in a nominal plant, $G_n(s)$, as it appears in Fig. 3. The nominal plant that has been computed considering the mean values of previous ranges described. With regard to variability, $W_u^a(s)$ is a weighting function that defines the bounds of the changes between all plants respect to the nominal ones, and $\Delta(s)$ is the uncertainty function that fulfills $\|\Delta(s)\| < 1$.
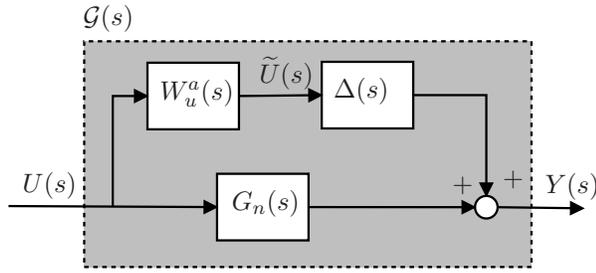
Fig. 3. Additive uncertainty model.

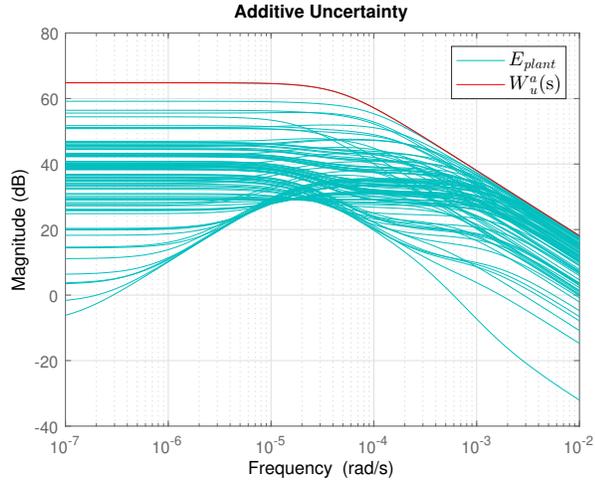

Fig. 5. Feedback controller for the uncertainty model.

Fig. 4. Second order $W_u^a(s)$ function (red) of the model uncertainty.

In order to obtain $W_u^a(s)$, the following procedure has been done:

1) Select a certain number of plants to perform the uncertainty. In this work, 2000 plants have been selected.
2) Determine the frequency range where to model the uncertainty. Looking Fig. 2 the bound selected is $[10^{-7}, 10^{-2}]$ rad/s.
3) Define a number of points logarithmically distributed along the bound defined in 2).
4) Define the set of plants with the frequency defined in 3).
5) Calculate the error (E_{plant}) of each new plant with respect to the nominal ones.
6) Obtain a function that bounds all errors of step 5).

Fig. 4 shows the corresponding $W_u^a(s)$ function that has been obtained following the procedure presented.

C. Controller design

Once the uncertainty has been modeled allowing the specification of all operating conditions, next step correspond to the design of the controller. The proposed controller follows a feedback configuration, that can be easily implemented by
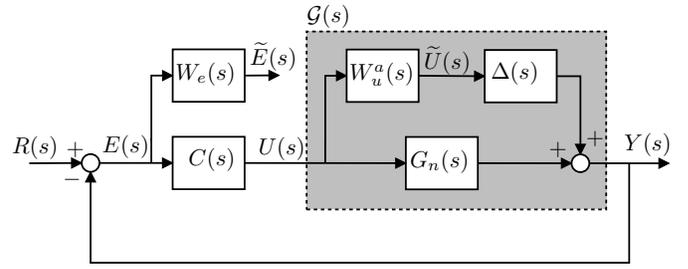
means of the previous functions defined as it is shown in Fig. 5.

As can be noticed, the new blocks correspond to the controller $C(s)$ and $W_e(s)$ that defines the system performance. The controller $C(s)$ can be designed in order to get a trade off between performance and stability, which can be established by means of the $|| \cdot ||_\infty$.

1) Performance condition: The performance of the system can be established in terms of the track error between the output voltage and the desired one, as well as the settling time. These parameters can be set using the sensitivity function of a system $S_n(s)$:

$$S_n(s) = \frac{E(s)}{R(s)} = \frac{1}{1 + C(s)G_n(s)}. \qquad (16)$$

Function $S_n(s)$ must be bounded selecting the proper performance parameters. A typical weighting function for $S_n(s)$ is [22]:

$$W_e(s) = \frac{1}{M_s} \left[\frac{s + M_s w_b}{s + \epsilon w_b} \right] \qquad (17)$$

where $1/M_s$ is the distance to the critical point (-1,0), and usually M_s takes a value between 1 and 2, parameters w_b is the bandwidth used to place the desired poles (and therefore the settling time) and ϵ is the desired steady-state error.

Thus, in order to obtain the desired performance, the following condition for the sensitivity function must be fulfilled:

$$|S_n(j\omega)| < \frac{1}{|W_e(j\omega)|}, \forall \omega \qquad (18)$$

Taking use of the $|| \cdot ||_\infty$, it can be rewritten as:

$$||W_e(s)S_n(s)||_\infty < 1. \qquad (19)$$

2) Stability condition: Once the performance condition has been formulated, next step corresponf to ensure the stability of the controlled system in closed-loop. Considering Fig. 5, the stability condition can be formulated using the $|| \cdot ||_\infty$ as:

$$||W_u^a(s)C(s)S_n(s)||_\infty < 1. \qquad (20)$$

3) Performance+Stability condition: Finally, by means of the $|| \cdot ||_\infty$ formulation, it is possible to develop a controller $C(s)$ that guarantees robust performance and stability by means of a mixed sensitivity problem based on conditions (19) and (20):

$$\min_{C(s)} \left\| \begin{array}{c} W_e(s)S_n(s) \\ W_u^a(s)C(s)S_n(s) \end{array} \right\|_\infty . \qquad (21)$$

IV. PID OPTIMIZED THROUGH PSO

A different methodology that can be used to design a controller for the VRFB system, is optimize a PID by means of a optimization problem. The procedure is based on define a cost function and some constraints that make possible to obtain the tuned PID parameters. There are different techniques such as the gradient descent method which are used to solve this type of convex problems. However, as the model presented imply some non-linearities, the optimization problem is transformed into a non-convex problem.

Considering this issue, in order to avoid solving local minima, a global optimization technique has been used, which consist on the Particle Swarm Optimization (PSO) method. A PSO is a technique used to optimize a problem computing iteratively a possible candidate considering a defined measure of quality.

For the case of the problem presented, the measure of quality selected is the tracking error, and the parameters to tune are the three proportional P, integral I and derivative D actions of the PID block implemented in the environment of Matlab-Simulink.

Therefore, the optimization problem can be expressed as:

$$\min_{\mathbf{p}} \quad \sum_{k=1}^{n_k} |V_{ref}(k \cdot T_s) - V(k \cdot T_s)|$$

subject to

$$\dot{\boldsymbol{x}}(k \cdot T_s) = \mathbf{A}\boldsymbol{x}(k \cdot Ts) + \mathbf{b} \cdot j(k \cdot Ts)$$
$$+ \mathbf{B}\boldsymbol{x} \cdot (V_{ref}(k \cdot T_s) - V(k \cdot T_s)) \cdot C(s)$$
$$V(k \cdot T_s) = h\left(\boldsymbol{x}(k \cdot T_s), j(k \cdot T_s)\right)$$
$$\mathbf{c}\left(\mathbf{p}\right) \leq \mathbf{0}.$$

where n_k is the total number of points into which the experiment is exactly divided, k is a point of the experiment, T_s is the sample period of time between two consecutive points, V is the measured output voltage, $\hat{V}$ is the estimated one obtained from the optimization and $\mathbf{c}$ is the constraints set of the parameters $\mathbf{p}$ that must be tuned and constitute the PID controller $C(s)$ which has the following expression:

$$C(s) = P + \frac{I}{s} + \frac{sD}{1+s} \qquad (22)$$

In this work, the constraints set $\mathbf{c}$ is conformed by the lower and upper bounds of the PID parameters. The value of its bounds appear summarized in TABLE I.

TABLE I
PARAMETERS BOUNDS

Parameter	Lower bound	Upper bound
P	0	4
I	0.1	1.0
D	0	1.0

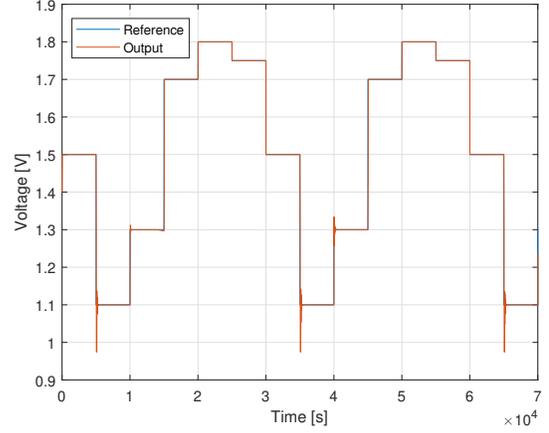

Fig. 6. Control of the voltage

V. RESULTS AND DISCUSSION

VI. COMPARATIVE EVALUATION

In order to evaluate the performance of both controllers designed, a deeper comparison have been done considering 4 different scenarios of a VRFB charging process.

1) Constant voltage demand at constant current
2) Constant voltage demand at variable current
3) Variable voltage demand at constant current
4) Variable voltage demand at variable current

VII. CONCLUSIONS

BLA BLA BLA

APPENDIX

The matrices $\mathbf{A}$, $\mathbf{B}$ and vector $\mathbf{b}$ are constants that only depend on the model parameters:

$$\mathbf{A} = \frac{2 \cdot s}{v_c \cdot d} \begin{pmatrix} -k_2 & 0 & -k_4 & -2k_5 & 0 & 0 & 0 & 0 \\ 0 & -k_3 & 2k_4 & 3k_5 & 0 & 0 & 0 & 0 \\ 3k_2 & 2k_3 & -k_4 & 0 & 0 & 0 & 0 & 0 \\ 2k_2 & -k_3 & 0 & -k_5 & 0 & 0 & 0 & 0 \\ 0 & 0 & 0 & 0 & 0 & 0 & 0 & 0 \\ 0 & 0 & 0 & 0 & 0 & 0 & 0 & 0 \\ 0 & 0 & 0 & 0 & 0 & 0 & 0 & 0 \\ 0 & 0 & 0 & 0 & 0 & 0 & 0 & 0 \end{pmatrix}$$
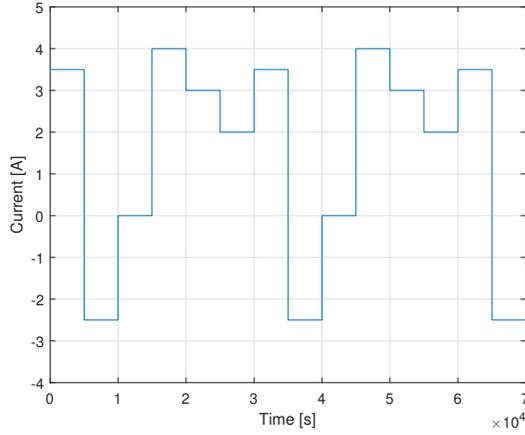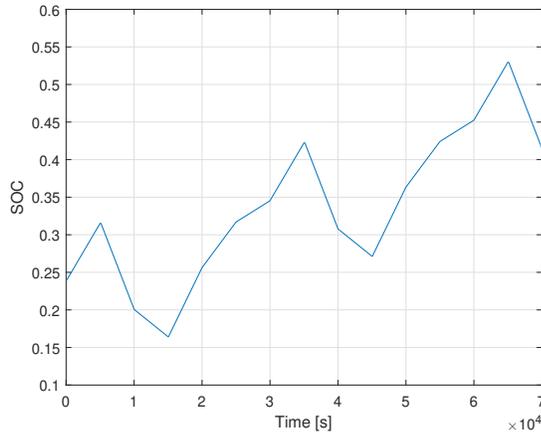
Fig. 7. Current behaviour

Fig. 8. SOC monitoring

$$\mathbf{B} = \begin{pmatrix} -\frac{2}{v_c} & 0 & 0 & 0 & \frac{2}{v_c} & 0 & 0 & 0 \\ 0 & -\frac{2}{v_c} & 0 & 0 & 0 & \frac{2}{v_c} & 0 & 0 \\ 0 & 0 & 0 & 0 & 0 & 0 & 0 & 0 \\ 0 & 0 & 0 & 0 & 0 & 0 & 0 & 0 \\ \frac{1}{v_t} & 0 & 0 & 0 & -\frac{1}{v_t} & 0 & 0 & 0 \\ 0 & \frac{1}{v_t} & 0 & 0 & 0 & -\frac{1}{v_t} & 0 & 0 \\ 0 & 0 & \frac{1}{v_t} & 0 & 0 & 0 & -\frac{1}{v_t} & 0 \\ 0 & 0 & 0 & \frac{1}{v_t} & 0 & 0 & 0 & -\frac{1}{v_t} \end{pmatrix}$$

$$\mathbf{b} = \frac{2s_e}{Fv_c} \left(1, -1, -1, 1, 0, 0, 0, 0 \right)^T$$

REFERENCES

[1] Eurostat, "Wind and water provide most renewable electricity; solar is the fastest-growing energy source," (Accessed 14.04.2021). [Online]. Available: https://ec.europa.eu/eurostat/statistics-explained

[2] G. Coppez, S. Chowdhury, and S. Chowdhury, "The importance of energy storage in renewable power generation: A review," *45th International Universities Power Engineering Conference UPEC2010*, pp. 1–5, 01 2010.

[3] P. Alotto, M. Guarnieri, F. Moro, and A. Stella, "Redox flow batteries for large scale energy storage," in *2012 IEEE International Energy Conference and Exhibition (ENERGYCON)*, pp. 293–298, 2012.

[4] S. Skarvelis-Kazakos, B. A. Giwa, and D. Hall, "Microgrid power balancing with redox flow batteries," in *IEEE PES Innovative Smart Grid Technologies, Europe*, pp. 1–6, 2014.

[5] M. Skyllas-Kazacos, M. Rychcik, R. G. Robins, A. G. Fane, and M. A. Green, "New all-vanadium redox flow cell," in *Journal of The Electrochemical Society*, vol. 133, no. 5, p. 1057, 1986.

[6] A. Cunha, J. Martins, N. Rodrigues, and F. P. Brito, "Vanadium redox flow batteries: a technology review," *International Journal of Energy Research*, vol. 39, no. 7, pp. 889–918, 2015.

[7] A. Clemente and R. Costa-Castelló, "Redox flow batteries: A literature review oriented to automatic control," *Energies*, vol. 13, p. 4514, 09 2020.

[8] C. Blanc and A. Rufer, "Optimization of the operating point of a vanadium redox flow battery," in *2009 IEEE Energy Conversion Congress and Exposition*, pp. 2600–2605, 2009.

[9] T. Takahashi and B. Sato, "Battery pack and charging method," U.S. Patent 12/725,109, 2010.

[10] L. Eifert, Z. Jusys, R. Behm, and R. Zeis, "Side reactions and stability of pre-treated carbon felt electrodes for vanadium redox flow batteries: A dems study," *Carbon*, vol. 158, pp. 580–587, 2020.

[11] C.-N. Sun, F. Delnick, L. Baggetto, G. Veith, and T. Zawodzinski, "Hydrogen evolution at the negative electrode of the all-vanadium redox flow batteries," *Journal of Power Sources*, vol. 248, p. 560, 10 2013.

[12] A. Clemente, G. A. Ramos, and R. Costa-Castelló, "Voltage H_∞ control of a vanadium redox flow battery," *Electronics*, vol. 9, no. 10, 2020.

[13] B. Xiong, J. Zhao, Y. Su, Z. Wei, and M. Skyllas-Kazacos, "State of charge estimation of vanadium redox flow battery based on sliding mode observer and dynamic model including capacity fading factor," *IEEE Transactions on Sustainable Energy*, vol. 8, no. 4, pp. 1658–1667, 2017.

[14] C. Blanc, "Modeling of a vanadium redox flow battery electricity storage system," *Doctoral Thesis*, 01 2009.

[15] J.-Y. Chen, C.-L. Hsieh, N.-Y. Hsu, Y.-S. Chou, and Y.-S. Chen, "Determining the limiting current density of vanadium redox flow batteries," *Energies*, vol. 7, no. 9, pp. 5863–5873, 2014.

[16] R. Badrinarayanan, J. Zhao, K. Tseng, and M. Skyllas-Kazacos, "Extended dynamic model for ion diffusion in all-vanadium redox flow battery including the effects of temperature and bulk electrolyte transfer," *Journal of Power Sources*, vol. 270, pp. 576–586, 2014.

[17] A. Tang, J. Bao, and M. Skyllas-Kazacos, "Dynamic modelling of the effects of ion diffusion and side reactions on the capacity loss for vanadium redox flow battery," *Journal of Power Sources*, vol. 196, no. 24, pp. 10 737–10 747, 2011.

[18] S. K. Murthy, A. K. Sharma, C. Choo, and E. Birgersson, "Analysis of concentration overpotential in an all-vanadium redox flow battery," *Journal of The Electrochemical Society*, vol. 165, no. 9, pp. A1746–A1752, 2018.

[19] R. Badrinarayanan, J. Zhao, K. Tseng, and M. Skyllas-Kazacos, "Extended dynamic model for ion diffusion in all-vanadium redox flow battery including the effects of temperature and bulk electrolyte transfer," *Journal of Power Sources*, vol. 270, pp. 576–586, 2014.

[20] A. Clemente, M. Montiel, F. Barreras, A. Lozano, and R. Costa-Castellò, "Vanadium redox flow battery state of charge estimation using a concentration model and a sliding mode observer," *IEEE Access*, 05 2021.

[21] R. Sánchez-Peña and M. Sznaier, *Robust Systems Theory and Applications*. Wiley, 08 1998.

[22] R. S. Sánchez-Peña and M. Sznaier, *Robust Systems Theory and Applications*, ser. Adaptive and Learning Systems for Signal Processing, Communications and Control Series. Wiley-Interscience, Aug. 1998.